ORP-42447
Revision 0

Crystallization in Multicomponent Glasses

Prepared for the U.S. Department of Energy
Assistant Secretary for Environmental Management

Office of River Protection

P.O. Box 450
Richland, Washington 99352

ORP-42447
Revision 0

Crystallization in Multicomponent Glasses

P. Hrma
Pacific Northwest National Laboratory

A. A. Kruger
Department of Energy - Office of River Protection

Date Published
October 2009

DOE-ORP
Richland, WA

Published in
Journal of Non-Crystalline Solids

Prepared for the U.S. Department of Energy
Assistant Secretary for Environmental Management

P.O. Box 450
Richland, Washington 99352


Release Approval

10/07/2009
Date

Crystallization in multicomponent glasses

Pavel Hrma

Pacific Northwest National Laboratory, Richland, Washington

pavel.hrma@pnl.gov

Abstract

In glass processing situations involving glass crystallization, various crystalline forms nucleate, grow, and dissolve, typically in a nonuniform temperature field of molten glass subjected to convection. Nuclear waste glasses are remarkable examples of multicomponent vitrified mixtures involving partial crystallization. In the glass melter, crystals form and dissolve during batch-to-glass conversion, melter processing, and product cooling. Crystals often agglomerate and sink, and they may settle at the melter bottom. Within the body of cooling glass, multiple phases crystallize in a non-uniform time-dependent temperature field. Self-organizing periodic distribution (the Liesegnang effect) is common. Various crystallization phenomena that occur in glassmaking are reviewed.

Key words: crystallization, nonequilibrium conditions, nuclear waste glasses, agglomeration, settling

1. Introduction

Almost all commercial glasses, all waste glasses and geological glasses, and many specialty glasses are multicomponent. Crystals that grow or dissolve in such glasses have a different composition from the matrix glass, and they often grow and dissolve in a moving melt (or crystals move through the melt by buoyancy) at a changing temperature.

Examples of crystallinity behavior given in this review are based on studies undertaken with glasses designed for the vitrification of nuclear waste at Hanford. Nuclear waste glasses contain most of the chemical elements, and the final product is usually formed into large bodies in which the internal portion of the glass cools slowly. These circumstances are conducive to crystallization, which

appears inevitable, unless the waste fraction in the glass is uneconomically low. Therefore, crystallization is nearly ubiquitous in waste glasses and as such needs to be understood to avoid undesirable impacts of crystal formation on glass processing and to characterize its impact on the final product. Fortunately, crystallinity only rarely compromises the waste glass quality, i.e., its chemical durability, in an unacceptable degree.

2. Batch-to-glass conversion [1-8]

Some, if not most, of the components of glass batches are crystalline or amorphous that turn into crystalline phases at elevated temperatures. Crystalline batch materials are of two types: ionic salts (carbonates, nitrates, sulfates, halides, etc.) and simple or complex oxides, hydroxides, or oxyhydrates (silica, silicates, iron oxide and hydroxide, alumina, etc.). Ionic salts melt early on heating, forming low-temperature eutectics. Carbonates and nitrates then react with boron oxide, silica, and other components, releasing copious amounts of gas, whereas sulfates and halides partly dissolve in the glass-forming melt, partly evaporate or decompose, and partly segregate. In batches with a large content of iron, a fraction of iron oxide and hydroxide may turn into hematite that turns to magnetite when Fe(III) begins to reduce to Fe(II) at higher temperatures. Magnetite extracts from the melt other spinel-forming oxides, such as NiO and Cr_2O_3, becoming a solid solution of magnetite, trevorite, chromite, and other simple spinels. As the temperature increases, spinel crystals eventually partly or fully dissolve in the glass-forming melt. Some of these features can be seen in Figure 1.

If alumina is present in the form of gibbsite or boehmite, it reacts with the early melt without forming crystals, but may precipitate as nepheline or a sodalite type phase when silica begins to dissolve. Both these crystalline forms dissolve in the glass-forming melt as the temperature rises. If alumina is present in the form of corundum, nepheline can be an intermediate crystalline phase. Similarly, zirconia and zirconium nitrate may first form zirconium silicate, sodium-zirconium silicate, or rare-earth zirconates before it fully dissolves in molten glass. Nuclear wastes typically contain oxides of noble metals Pd, Rh, and Ru. Their salts are initially a part of the ionic-salt melt from which they may precipitate in the form of metals or oxides and partly dissolve in the glass-forming melt.

Needle-shaped crystals of RuO_2 do not redissolve in the melt and may interact with spinel as seen in Figure 2 (see also Section 8).

Quartz is usually added as the source of silica, a major glass former. The size of its particles is of a crucial importance. Small particles (< 50 μm) dissolve too early, producing a highly-viscous melt that tends to create foam. When large quartz particles (>100 μm) dissolve, the silica-rich layers of melt around them impinge on each other, usually pushed by gas bubbles moving through the less viscous melt. This results in the formation of slowly dissolving clusters of several silica particles.

Refractory oxides (SiO_2, Al_2O_3, RuO_2, ZrO_2) dissolve, and intermediate crystalline phases form and eventually dissolve as an integral part of batch-to-glass conversion. In case of the waste-glass processing in a continuous melter, some of these phases may persist, interfere with processing, and even shorten the melter lifetime (see Section 6). Some commercial glasses are also prone to crystallization. For example, wollastonite, devitrite, or cristobalite may form in float glass.

3. Phase equilibria [9,10]

Crystallization and dissolution phenomena, whether during the batch-to-glass conversion or during slow cooling of glass, proceed, by their very nature, far from equilibrium. However, the knowledge of equilibria is important because it is the distance from equilibrium (in the composition space) that drives the process. For any glass composition, the liquidus temperature (T_L) is the ultimate equilibrium as far as the primary crystalline phase is concerned. Above T_L, crystals can only dissolve whereas crystals can either dissolve or grow below T_L, depending on whether the melt is oversaturated or undersaturated with the crystalline material.

Because the highly multicomponent glasses are crowded with components and, as a result, each component is confined to a limited, even narrow, range of concentration, glass properties can generally be approximated as linear fictions or mass of mol fractions of glass components fitted to a manageable amount of experimental data. This linearity greatly simplifies the formulation of glasses that contain as high a fraction of waste as possible and possess properties, such as viscosity, electrical conductivity, and chemical durability, compatible with processing technology and regulatory

requirements. Thus for the T_L as a function of composition, it is sufficient to obtain a coefficient for each major component, such that

$$T_L = \sum_{i=1}^{N} T_i x_i \tag{1}$$

where T_i is the i-th component coefficient, x_i is the i-th component mass or mole fraction (or the atomic fraction of the i-th ion), and N is the number of liquidus-affecting components. To measure T_is, the experiments are often designed in such a way that T_L is measured for glasses with a component added to or removed from, one at a time, a centroid composition. Thus, four compositions usually suffice for each component to obtain a reliable value of T_i and to verify the assumption of linearity. Most of the glass components increase the T_L of spinel, but alkali and B_2O_3 decrease it. B_2O_3 also decreases the T_L of nepheline, a highly undesirable crystalline species in the waste glass (see Section 8).

When T_is for magnetite-trevorite-chromite spinel were expressed per mole fractions of cations, they correlated with the ionic potentials, $P_i = z_i/r_i$, where z_i is the ionic charge and r_i the ionic radius, forming two branches in the shape of Λ as seen in Figure 3 [11]. This allows estimating T_is also for glass components for which the composition variation has not been performed. The only exceptions are Cr, Ni, and Mn, whose T_is do not follow the Λ pattern.

At a temperature below T_L, the equilibrium between the crystalline phase and the melt can be expressed in the form of a pseudo-binary mixture in which the crystalline material forms one component and the melt the other. An example of such a binary phase diagram is shown in Figure 4 for the crystalline phase of spinel. The ideal-solution equation,

$$C_0 = C_{\max}\left\{1 - \exp\left[-B_L\left(\frac{1}{T} - \frac{1}{T_L}\right)\right]\right\} \tag{2}$$

where C_0 is the equilibrium mass fraction of crystalline phase in the mixture, and C_{max} and B_L are temperature-independent coefficients, represents the data well over the temperature interval of more than 300°C below T_L. Note that C_0 is a function of temperature and, therefore, the degree of conversion, expressed as $\xi = (C_0 - C)/(C_0 - C_i)$ where the subscript i denotes the initial value, cannot be considered as an independent variable in nonisothermal processes (a commonly committed oversight) unless C_0 is nearly constant (at a temperature far bellow T_L).

4. Nucleation [10]

Certain crystals do not form unless the glass is first annealed at a lower temperature to generate nuclei. Other crystals, such as aegirine ($NaFeSi_2O_6$), form at a constant temperature only after some incubation time and thus may not form easily during cooling [12]. Nepheline nuclei exist even at temperatures above the T_L and thus precipitate rapidly as soon as the temperature drops below the liquidus. Spinel exhibits a similar behavior. As Figure 5 shows, ~10 crystals per mm^3 formed spontaneously below T_L. When the melt was quenched to various temperatures below T_L, the number of spinel nuclei increased by orders of magnitude until it reached a maximum of ~10^8 crystals per mm^3 at ~500°C.

Since $C = \zeta n_S a^3 \rho$, where ζ is the shape factor, n_S is the crystal number density, a is the crystal size, and ρ is the crystal density—the smaller the number of crystals nucleated, the larger the crystals grow. Large spinel crystals, ~100 μm in size, would not dissolve during the residence time of the melt in a waste glass melter, and, having a density twice as high as that of the glass, would tend to settle to the melter bottom. To decrease the crystal size to 1 μm, it is necessary to increase n_S from 10 mm^{-3} to 10^7 mm^{-3}. This would not happen during a slow cooling. As Figure 5 indicates, n_S is large when noble metals that provide heterogeneous nuclei are present. Fortunately, Ru, Rh, and Pa are common in nuclear wastes, and thus all undissolved spinel is likely to be discharged from the melter (see Section 8).

5. Crystal growth/dissolution rate [10,12,13]

Both the growth rate and the dissolution rate of a crystal in a multicomponent glass are commonly controlled by diffusion, and thus the growth/dissolution rate equals the diffusion mass flux at the interface. To be exact, the moving boundary must also be considered, but we omit this effect here for simplicity (also, we ignore other secondary phenomena, such as the impact of multicomponent diffusion on the composition at the interface or the changing solid composition if the crystal is a solid solution). Thus, $j = \rho da/dt$, where j is the mass flux, and t is the time. By the Fick's law, $j = -\rho D\, \partial C/\partial r|_{r=a}$, where D is the effective binary diffusion coefficient, and r is the radial coordinate. Alternatively, $da/dt = -(D/\delta)(C - C_0)$, where δ is the diffusion boundary layer thickness, and C_0 is the concentration of the crystalline material at the solid-melt interface. The mass transfer coefficient, k, is defined as $k = D/\delta$.

Under common circumstances, the melt at the interface is saturated, and thus C_0 is the equilibrium concentration, which is, by Equation (2), a function of temperature. As the diffusion layers around crystals grow, they eventually impinge at each other, resulting in the decrease of C, and, hence, the rate of crystallization. Various approximations exist for estimating this effect. For a motionless system at a constant temperature, a useful approximation is known as the Kolmogorov-Mehl-Johnson-Avrami (KMJA) equation [14],

$$\frac{C_0 - C}{C_0 - C_i} = \exp\left[-(k_A t)^n\right] \tag{3}$$

where k_A is the rate coefficient, and n is the Avrami exponent. Figure 6 demonstrates that this equation is indeed en excellent approximation of the observed behavior of spinel over a wide range of time and temperatures. Here Equation (2) was used for C_0. The Arrhenius function was used for k_A:

$$k_A = k_{A0} \exp(-B_A / T) \tag{4}$$

where k_{A0} and B_A are temperature-independent coefficients. A similar diagram was constructed for nepheline and aegirine (acmite). Note that the temperature-dependence of C_0 cannot be ignored even for a constant temperature process. Equation (3) cannot be used for a nonisothermal situation. For those, by the principle of frame-independence, the rate can only be a function of the frame-independent variables (see Section 6).

The KMJA equation is applicable only to non-convective situations. When the melt flows or crystals move, the diffusion layers are suppressed, and the bulk concentration changes faster. This situation is better addressed by the Hixson-Crowell equation [15],

$$\frac{da}{dt} = 2n_S k_H \left(a_0^3 - a^3\right) \tag{5}$$

where k_H is the rate coefficient. The Hixson-Crowell equation should be applied also when densely populated crystals fall in otherwise quiescent melt unless they are so small that their velocity has a negligible effect on their growth or dissolution.

Levich analyzed how a falling individual crystal dissolves [16]. He used the boundary-layer theory, obtaining

$$\delta = \frac{1.15\left(\theta - \dfrac{\sin 2\theta}{2}\right)^{1/3}}{\sin\theta}\left(\frac{Da^2}{3u}\right)^{1/3} \tag{6}$$

where θ is an angular coordinate, and u is the velocity of a falling particle. This equation was verified with the images of spinel crystals falling in the melt held at a temperature above the liquidus. As seen in Figure 7, the crystals were leaving behind a comet-like tale of colored glass, the shape of which was well described by Equation (6). Moreover, the measured horizontal concentration distribution and dissolution rate resulted in a value of D similar to that found in the literature.

The rate of growth and dissolution of spinel crystals is plotted in Figure 8 as a function of temperature. As the temperature increases, the growth rate increases to a maximum and then decreases to zero at T_L. Note that the dissolution rate does not drop to zero at T_L because crystals can dissolve at $T < T_L$ if $C > C_0$.

6. Nonisothermal conditions

As mentioned in a previous section, Equation (3) does not apply to a nonisothermal process. A frame-indifferent differential equation that yields Equation (3) for T = const. has the form [10]

$$\frac{dC}{dt} = nk_A(C_0 - C)\left[-\ln\left(\frac{C_0 - C}{C_0 - C_i}\right)\right]^{(n-1)/n} \tag{7}$$

For the constant cooling rate, $dT/dt = -\Phi$, we have $dC/dt = -\Phi dC/dT$, and Equation (7) can be solved numerically. The solution is expressed in Figure 9 as C versus t and C versus T with Φ as a parameter [17]. As expected, it shows that little crystallinity is produced at a fast cooling rate, and an extremely slow cooling rate results in nearly equilibrium crystallinity unless the temperature is close to the glass-transition interval (interestingly, nepheline precipitation does not stop at the T_g of the original glass because the T_g of the matrix glass decreases, as nepheline, $NaAlSiO_4$, is depleting it from the SiO_4 and $NaAlO_4$ glass-forming structural units).

Figure 10 shows a time-temperature transformation diagram in which the C is mapped on a T-t plane. This diagram is valid solely for the cooling represented by a linear function $T = T_L - \Phi t$, where t is measured from the moment at which the decreasing temperature (at a constant rate, Φ) reached T_L. This fashionable type of presenting crystallization is commonly constructed from isothermally obtained data, and any conclusions drawn from such a diagram for nonisothermal crystallizations are potentially misleading.

The time-temperature history of a glass poured from the melter discharge to a waste glass canister can be simplified as consisting of five stages [17]: 1) the stream of the melt falls from the

melter discharge to the canister opening, 2) the melt flows from the point of impact towards the canister wall, 3) the melt rests on the top surface of the glass in the canister, 4) the top melt is covered by the subsequent layer, and 5) the glass cools down. The evolution of the temperature field during these stages was calculated using the Navier-Stokes and energy-balance equations and was also measured by a series of thermocouples during a canister-filling test. Thus, the spinel fraction distribution could be calculated using Equation (7). Figure 11 shows the result.

Spinel crystals that enter the all-electric melter from the batch floating on the melt surface are carried away from the batch-melt interface by the convective currents. Although the throughput convection is generally slow, the natural convection driven by buoyancy (as a result of temperature gradients) is fast and can be greatly enhanced by bubbling. Thus, spinel is subjected to velocity gradients and changing temperature. The distribution of spinel in the melter, both with respect to its crystal size and the mass fraction, was mathematically modeled. The model estimated the accumulation of spinel crystals in the melter caused by settling.

A similar model was developed for the crystals of RuO_2 [18]. The model predicted that the extremely small needles of RuO_2 cannot settle during the melter life time in any measurable amount. This, however, was at variance with pilot-scale experiments. The authors resolved the paradox by assuming that the crystals that come to some distance from the melter bottom are somehow trapped. However, the entrapment distance necessary for an agreement with experiment would be several times larger than the crystal size. The authors did not explain how this would be possible. However, as RuO_2 crystals are known to form large agglomerates [19-22] (an effect of densification in the shrinking pockets of molten salts during melting and the shear-flocculation mechanism in the circulating melt), the enhanced settling is probably a result of higher sinking velocity of the agglomerates. Even though the density of the agglomerates is lower than the density of crystals, their sizes can be sufficiently large to substantially increase the settling velocity (the Stokes velocity is proportional to the square of the particle size).

7. Dendritic growth and self-organization phenomena

The common shapes of crystals formed during slow cooling or at a constant temperature not far below the T_L are compact and determined by the particular crystallographic group. Thus, spinel forms regular octahedrons (Figure 12) that may group into agglomerates (Figure 13). Nepheline and baddeleyite crystals are displayed in Figure 14. If the melt is subjected to rapid cooling to a temperature at which the rate of growth is fast, the moving interface breaks through the thin diffusion layer, creating instability that leads to the formation of dendrites, as seen in Figure 15.
Spinel crystals may organize themselves into parallel layers, as seen in Figure 16. These layers are often bent and distorted by convection or by moving bubbles. They are a manifestation of the Liesegang phenomenon. When the temperature gradient moves through the melt, spinel crystallizes when the temperature decreases below T_L, and the diffusion of spinel components depletes the melt from them up to some distance. The new layer begins to crystallize when the temperature front reaches the undepleted mass. This can happen during cooling, for example, when the melt is poured from a crucible on a cold steel. This can also happen during reheat, for example, when the stream of the hot melt flows over a colder melt (Figure 16). Both dendritic growth and the Liesegang effect have been well understood and mathematically described in the literature.

8. Effect of crystallization on nuclear-waste-glass processing and on the waste-glass quality

Crystal settling is a potential problem regarding the performance and even the lifetime of a continuous waste-glass electric melter [23]. Figure 17 shows an optical micrograph of a thin section of a spinel sludge, the sample of which was retrieved from an experimental melter vitrifying simulated waste made without adding the noble metals. Spinel crystals grew large (~100 μm) and produced a layer of sludge within a relatively short melter run.

Spinel crystals that grow in the batch and reach the melt circulating in the melter are carried by convection either along the walls, or through the central region of the melter, or in the flow cells from the bubblers until they come close to the melter bottom. The velocity of crystal in melt is a superposition of the melt velocity and the Stokes velocity, $u = k_S \Delta\rho g a^2/\eta$, where k_S is the Stokes coefficient ($k_S = \sim 0.04$ for hindered settling of octahedrons), $\Delta\rho$ is the density difference between

spinel and melt, g is the acceleration due to gravity, and η is the melt viscosity. With $\Delta\rho \approx 2.5\times10^{3}$ kg·m^{-3}, $g \approx 10$ m·s^{-2}, $\eta \approx 10$ Pa·s, and $a \approx 10^{-4}$ m, we obtain $u \approx 1.3\times10^{-6}$ m·s^{-1} and with $a \approx 10^{-6}$ m, $u \approx 5\times10^{-10}$ m·s^{-1}. The rate of growth of the sludge layer is $U = uv_G/v_S$, where v_G and v_S are the spinel volume fraction in glass and in sludge, respectively. Based on samples from experimental melter runs, $v_S = \sim0.15$. With $v_G = 0.005$, we estimate $U \approx 3\times10^{-8}$ m·s^{-1} for 100-μm crystals and 3×10^{-12} m·s^{-1} for 1-μm crystals. Hence, 100-μm crystals would create 0.9-m sludge in 1 year in this extreme case. Spinel agglomerates would settle even faster. On the other hand, small crystals may totally dissolve while circulating in the melter. Even in the worst case of no dissolution, most of 1-μm crystals will not settle, leaving behind a minute 95-μm layer of sludge in 1 year. Spinel sludge, when formed, cannot be dissolved within a reasonable length of time because the melter bottom is relatively cold, and the sludge cannot be easily disturbed.

As mentioned in Sections 2 and 6, crystals of RuO_2 can also form sludge, with or without spinel. Needles of RuO_2 not only increase the resistance of the sludge against mechanical agitation, but also can distort the electric field in the melter because RuO_2 is electrically conductive.

Even more worrisome is the possibility of spinel settling within the melter discharge zone during the time of melter idling. Here not only the crystal size is important, but also the T_L; crystallinity can be eliminated if the temperature in the discharge zone is kept above the liquidus.

The chemical durability of a glass with crystals can be estimated as that of the matrix glass, the average composition of which can be obtained from the fraction and composition of the crystalline phases present [24]. This, however, disregards other effects that can increase the corrosion rate, such as the existence of diffusion layers around the crystals (these layers are more depleted of the crystal-forming components than the bulk glass), internal stresses associated with crystallization, the presence of cracks, water diffusion around the interfaces, crystallization-induced phase separation, etc. Fortunately, for the lack of nucleation, a long incubation time, and a slow growth, most of the crystalline forms do not actually occur during glass cooling, or they form in concentrations too low to

influence the rate of glass corrosion. The notable exception is nepheline, as has been mentioned in Section 6.

9. Conclusions

It is important to understand crystal growth and dissolution during continuous melting of nuclear waste glasses where the goal is to limit the settling of crystals in the melter, especially in its discharge. Various phenomena, such as metastable crystallization, heterogeneous nucleation, dendritic growth, and self-organizing precipitation, may occur and influence the impact of crystallization on glass processing and product quality (in some cases, crystallization can undesirably affect glass chemical durability).

The kinetics of crystal growth and dissolution in multicomponent glasses under both isothermal and nonisothermal conditions can only be properly represented by the rate equation of the form $dC/dt = f(C,T)$ where both thermodynamic and kinetic parameters (the equilibrium concentration, C_0, and the rate coefficient, k) are treated as functions of temperature.

Acknowledgment

Pacific Northwest National Laboratory (PNNL) is operated for the U.S. Department of Energy by Battelle under Contract DE-AC05-76RL01830. The author is grateful to the U.S. Department of Energy Office of River Protection for support of this review.

References

1. M. Cable, In: Glass: Science and Technology, D.R. Uhlmann and N.J. Kreidl (eds), Academic Press, 1984.
2. R. G. C. Beerkens, In: H. Loch, D. Krause (eds), Mathematical simulation in glass technology, Springer, 2002.
3. R. G. C. Beerkens, Silikaty, 52 (2008) 206.
4. P. Hrma, In: *Adv. in Fusion of Glass*, 10.1-18, *Am. Ceram. Soc.,* Westerville, Ohio, 1988.

5. P. Hrma, In: A Paul, *Chemistry of Glass*, Prentice Hall, London, 1990.
6. P. Hrma, J. Matyáš, D-S. Kim, In: *9th Biennial Int. Conf. On Nucl. Hazardous Waste Management, Spectrum '02*, American Nuclear Society, CD-ROM 2002.
7. B. Hanni, E. Pressley, J. V. Crum, K. B. C. Minister, D. Tran, P. Hrma, J. D. Vienna, *J. Mater. Res.* 20 (2005) 3346.
8. P. Hrma, D. E. Smith, J. Matyáš, J. D. Yeager, J. V. Jones, and E. N. Boulos, *Europ. J. Glass Sci Technol. B* 47 (2006) 64.
9. P. Hrma and A. A. Kruger, In: *Advanced Materials Research* 39-40 (2008) 633; online at http://www.scientific.net.
10. J. Alton, T.J. Plaisted, P. Hrma, J Non-Cryst Solids 311.(2002) 24.
11. J. D. Vienna, P. Hrma, J. V. Crum, and M. Mika, *J. Non-Cryst. Solids* 292 (2001) 1.
12. J.D. Vienna, P. Hrma, D.E. Smith, *Scientific Basis for Nuclear Waste Management* (Editors W.J. Gray and I.R. Triay), 465(1997) 17.
13. T.J. Menkhaus, P. Hrma, and H. Li, *Ceram. Trans.* 107 (2000) 461.
14. M. Avrami, *J. Chem. Phys.* 7 (1939) 1103; 8 (1940) 212; 9 (1941) 177.
15. A. W. Hixson, J. H. Crowell, *Ind. Eng. Chem.* 23 (1931) 923.
16. Levich, V.G., , *Physicochemical Hydrodynamics*, Prentice-Hall, New York, p. 80, 1962.
17. D. G. Casler, P. Hrma, *Mat. Res. Soc. Proc.* 556 (1999) 255.
18. W. Lutze, W. Gong, F. C. Perez-Cardenas, K. S. Matlack, I. L. Pegg, P. Schill, Europ. J. Glass Sci. Technol. A 48 (2007) 263.
19. G. Roth, S. Weisenburger, Role of noble metals in electrically heated ceramic waste glass melters, Forschungscentrum Karlsruhe Institut für Nucleare Entforschung, Karlsruhe, Germany, 2003.
20. C. Krause, B. Luckscheiter, J. Mat. Res. 6 (1991) 2535.
21. W.T. Cobb, P. Hrma, Ceram. Trans. 23 (1991) 233.
22. M. F. Cooper, M. L. Elliott, L. L. Eyler, C. J. Freeman, J. J. Higginson, L. A. Mahoney, M. R. Powell, Research-scale melter test report, PNL-9428, Pacific Northwest Laboratory, Richland, Washington, 1994.

23. P. Hrma, J. Alton, J. Klouzek, J. Matyas, M. Mika, L. Nemec, T.J. Plaisted, P. Schill, M. Trochta, Waste Manag. '01, University of Arizona, Tucson, Arizona, 2001.

24. B. J. Riley, P. Hrma, J. A. Rosario, J. D. Vienna, *Ceram. Trans.* 132 (2002) 257-265.

Figure Captions

Figure 1. Decomposition of sodium nitrate, dissolution of quartz, and formation and subsequent dissolution of spinel and sodalite during heating (at 4°C/min) of a simulated nuclear waste batch.

Figure 2. Spinel crystals interacting with RuO_2 needles. The central spinel crystal is ~25 μm in size.

Figure 3. Component coefficients of T_L, defined in Equation (1) and expressed per atomic fractions, versus ionic potentials (P_i) of the prevailing redox state of the ions.

Figure 4. Equilibrium concentration of spinel (in terms of mass%) in a simplified simulated nuclear waste glass. The line fitted to data represents the ideal solution Equation (2).

Figure 5. The spinel nucleation density, n_S, versus temperature in a simplified nuclear waste glass without (solid points) and with (open points) an addition of a noble metal (0.1 mass% of Pt).

Figure 6. Spinel fraction, in mass%, versus temperature and time (a parameter) during isothermal heat treatment of a simplified nuclear waste glass. The lines represent Equations (2) to (4) fitted to data.

Figure 7. An optical micrograph of a falling and dissolving crystal of spinel (~20 μm in diameter) in a simplified simulated nuclear waste glass.

Figure 8. Growth and dissolution rate of spinel in a simplified simulated nuclear waste glass versus temperature.

Figure 9. Spinel concentration (as a mass fraction) versus time and temperature during cooling at a constant rate.

Figure 10. Time-temperature transformation plot for spinel precipitating from molten glass at a constant rate of cooling. This diagram presents the same relationship as those in Figure 9.

Figure 11. Spinel volume fraction versus radial coordinate, r, in the cylindrical canister of the internal radius R at the ends of the five stages described in the text.

Figure 12. A typical octahedron of a spinel crystal in a simulated nuclear waste glass. The octahedron edges are 55 μm long.

Figure 13. An aggregate of spinel crystals in a simulated nuclear waste glass and a 100-μm bar.

Figure 14. Crystals of nepheline ($NaAlSiO_4$) , left, and baddeleyite (ZrO_2), right, in a simulated nuclear waste glass. The large nepheline crystal is 200×300 μm and sizes of larger baddeleyite crystals are ~20 μm.

Figure 15. Spinel dendrites in a simulated nuclear waste glass.

Figure 16. Spinel crystals in a simulated nuclear waste glass poured into a canister. Large crystals nucleated during pouring, and the small crystals, self-organized into parallel layers (here disturbed by a moving bubble), formed when hot glass reheated a cooler glass below.

Figure 17. Optical image of a thin section through a spinel sludge taken from an experimental waste glass melter (the dendrites in the middle top are metallic silver).

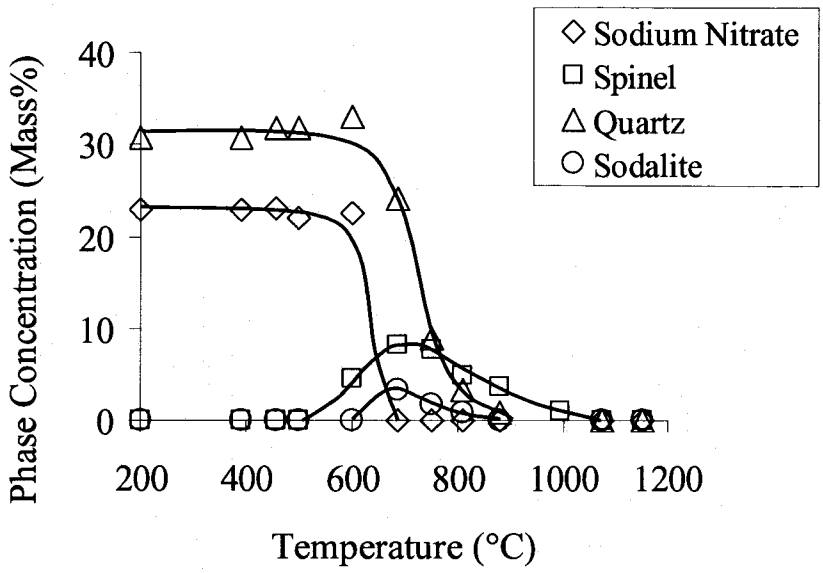
Sodium Nitrate
Spinel
Quartz
Sodalite
Phase Concentration (Mass%)
40
30
20
10
0
200
400
600
800
1000
1200
Temperature (°C)

Figure 1.

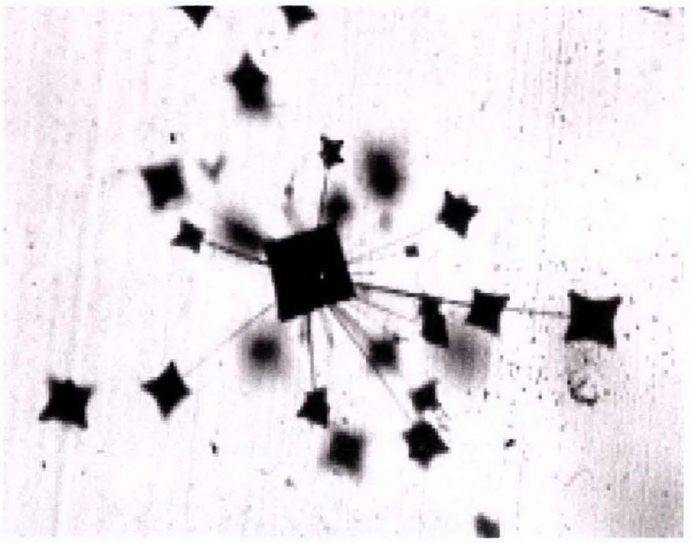

Figure 2.

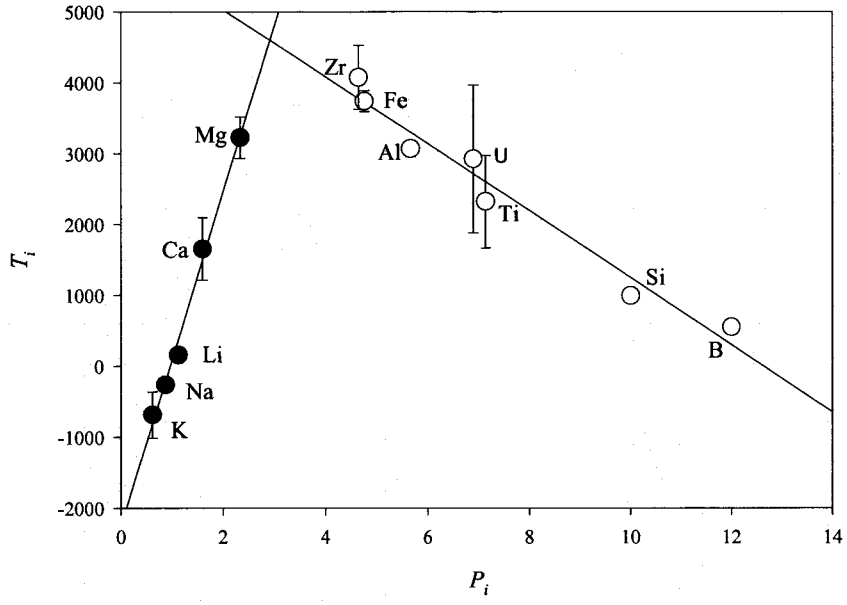
5000
4000
3000
2000
1000
0
-1000
-2000
0
2
4
6
8
10
12
14
T_i
P_i
Zr
Fe
Mg
Al
U
Ti
Ca
Si
B
Li
Na
K

Figure 3.

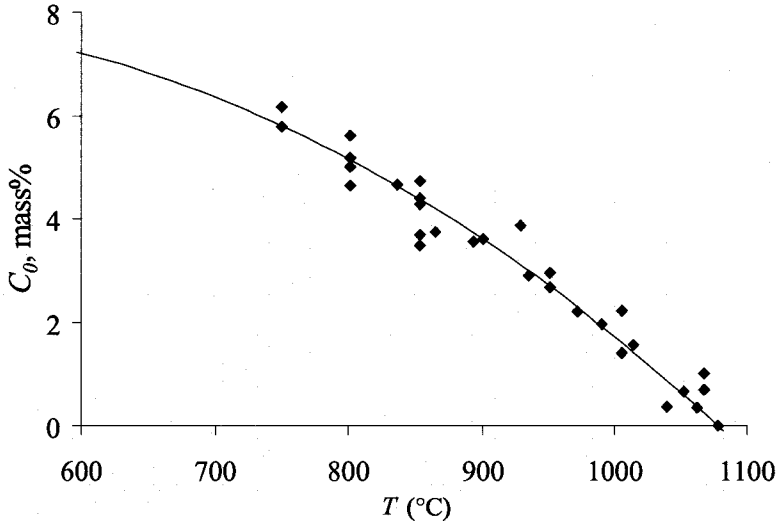

Figure 4.

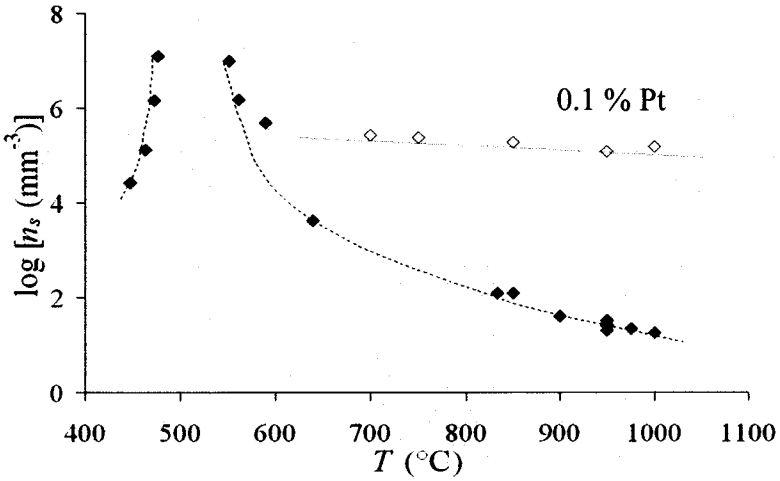

Figure 5.

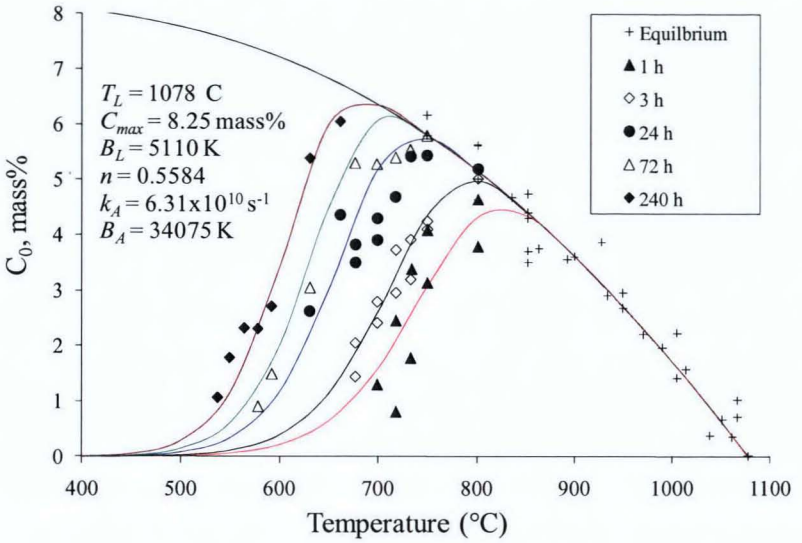
$T_L = 1078$ C
$C_{max} = 8.25$ mass%
$B_L = 5110$ K
$n = 0.5584$
$k_A = 6.31 \times 10^{10}$ s^{-1}
$B_A = 34075$ K
+ Equilbrium
▲ 1 h
◇ 3 h
● 24 h
△ 72 h
◆ 240 h
C_0, mass%
Temperature (°C)
0
1
2
3
4
5
6
7
8
400
500
600
700
800
900
1000
1100

Figure 6.

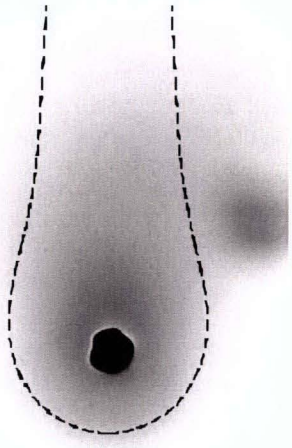

Figure 7.

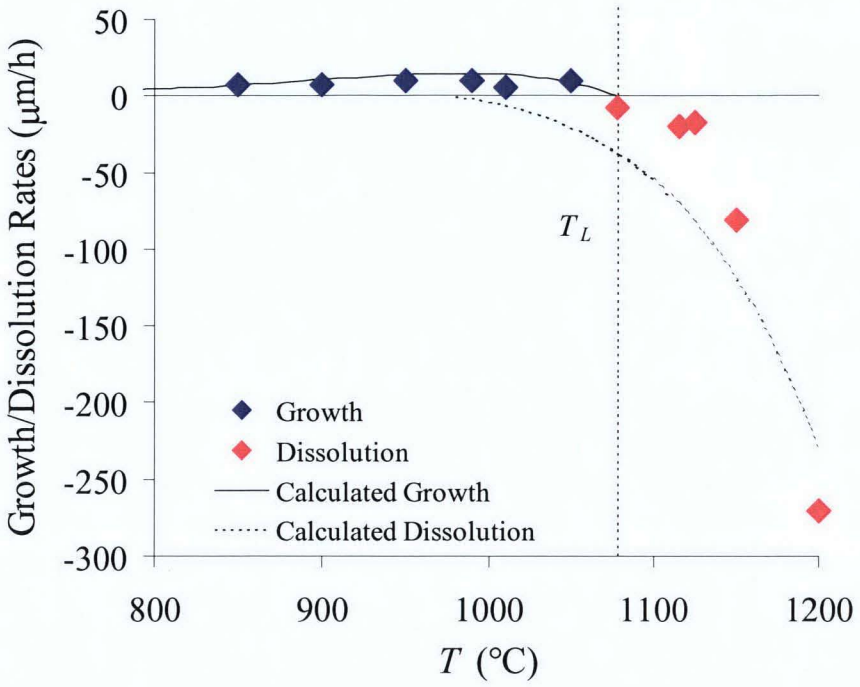
50
0
-50
-100
-150
-200
-250
-300
Growth/Dissolution Rates (μm/h)
T_L
Growth
Dissolution
Calculated Growth
Calculated Dissolution
800
900
1000
1100
1200
T (°C)

Figure 8.

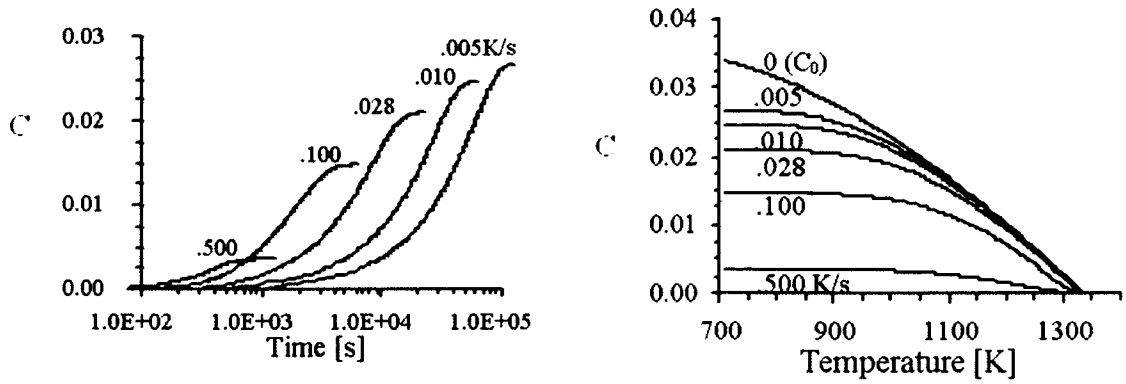
0.03
0.02
0.01
0.00
C
.005K/s
.010
.028
.100
.500
1.0E+02
1.0E+03
1.0E+04
1.0E+05
Time [s]
0.04
0.03
0.02
0.01
0.00
C
0 (C0)
.005
.010
.028
.100
500 K/s
700
900
1100
1300
Temperature [K]

Figure 9.

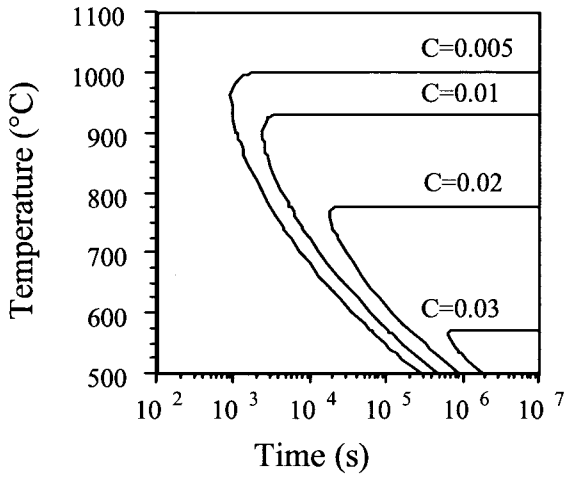
1100
1000
900
800
700
600
500
Temperature (°C)
C=0.005
C=0.01
C=0.02
C=0.03
10 2
10 3
10 4
10 5
10 6
10 7
Time (s)

Figure 10.

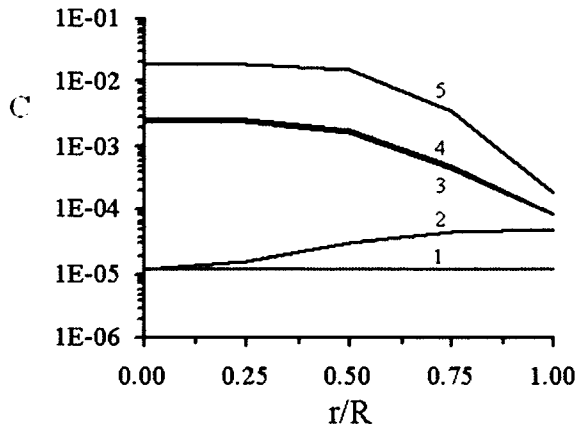

Figure 11.

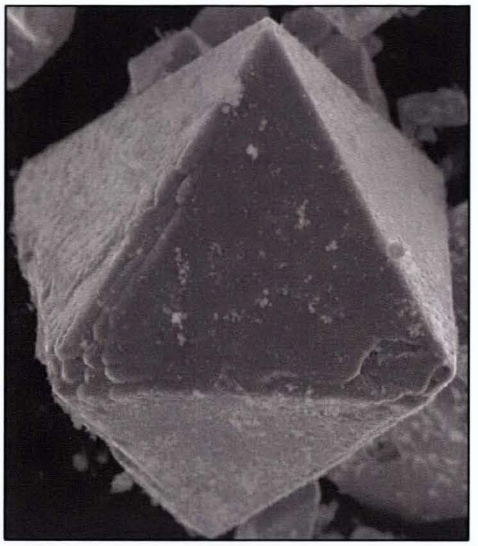

Figure 12.

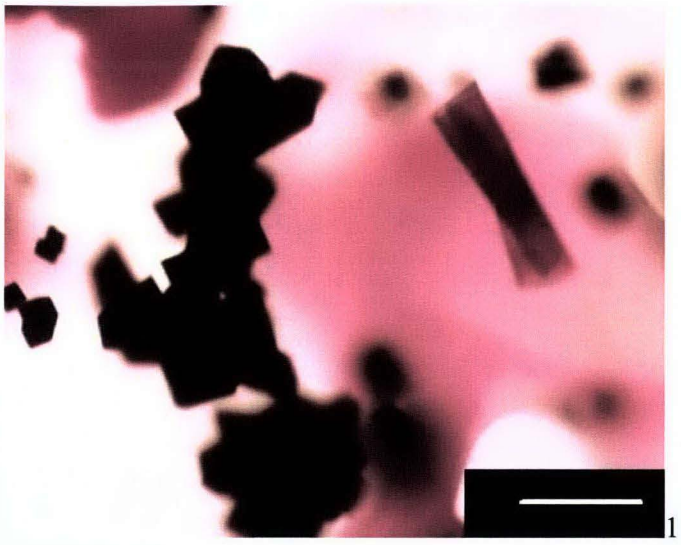

Figure 13.

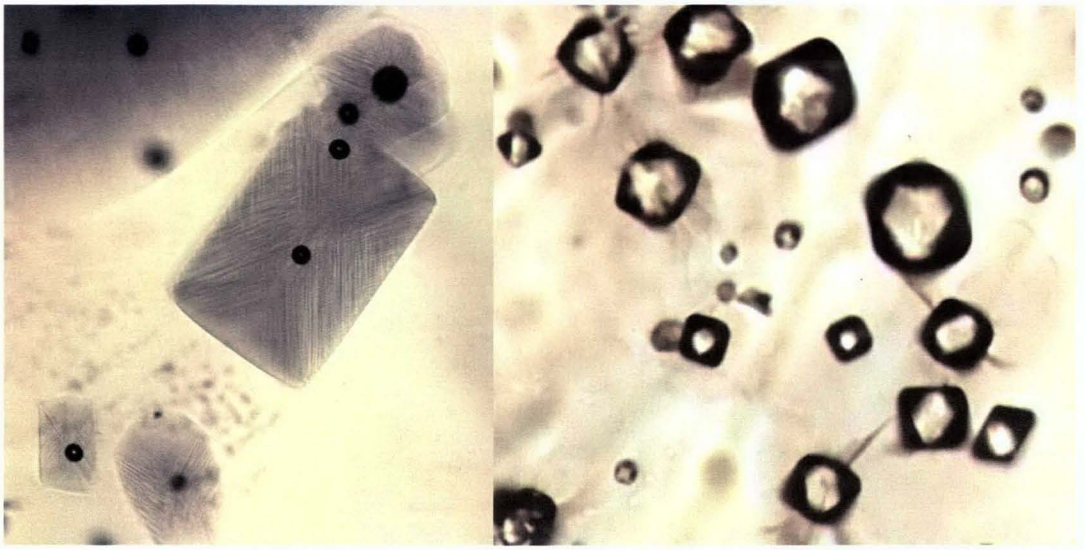

Figure 14.

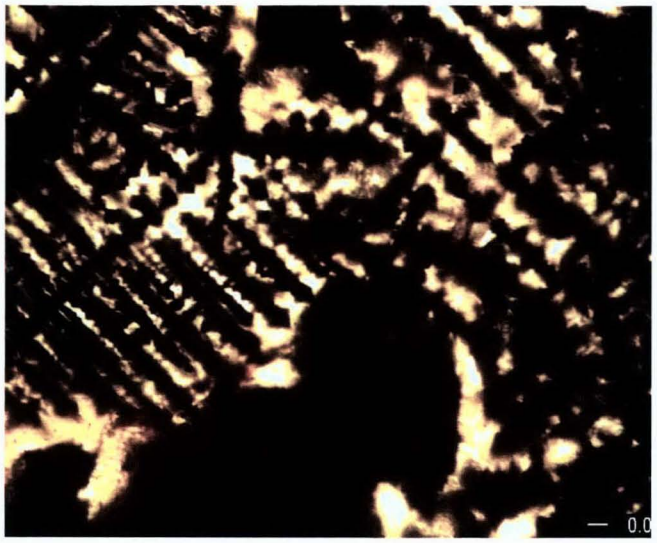

Figure 15.

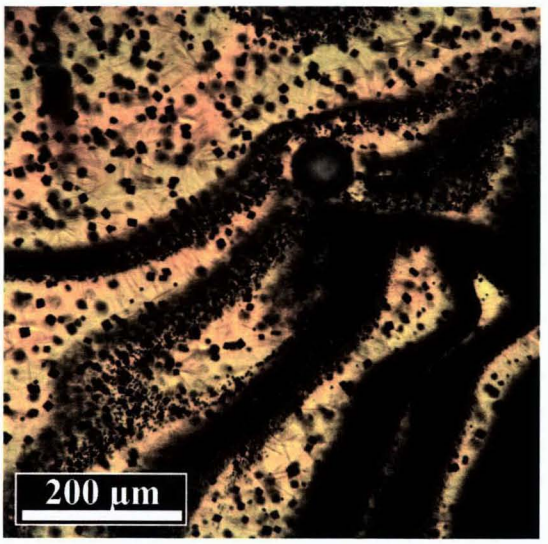

Figure 16.

Figure 17.